




ARTICLE OPEN



High performance flexible Sn-Pb mixed perovskite solar cells enabled by a crosslinking additive

Ya Li¹, Suhao Yan¹, Jiupeng Cao¹ [✉], Haoyu Chen¹, Bingxu Liu¹, Jiankai Xie¹, Yuting Shu¹, Fangfang Wang¹ [✉], Aifei Wang¹, Jingjin Dong¹ and Tianshi Qin¹ [✉]

Flexible perovskite solar cells (PSCs) have drawn increasing attention due to their promising applications for wearable electronics and aerospace applications. However, the efficiency and stability of flexible PSCs still lag behind their rigid counterparts. Here, we use N,N-dimethyl acrylamide (DMAA) to in situ synthesize cross-linking polymer for flexible Sn–Pb mixed PSCs. DMAA can gather at grain boundary as a scaffold to regulate the crystallization of perovskite and reduce defects. The rigid and flexible Sn–Pb mixed PSCs showed efficiencies of 16.44% and 15.44%, respectively. In addition, the flexible Sn–Pb mixed PSCs demonstrated excellent bending durability, which retained over 80% of the original efficiency after 5000 bending cycles at a radius of 5 mm.

npj Flexible Electronics (2023)7:18; <https://doi.org/10.1038/s41528-023-00253-4>

INTRODUCTION

Organic–inorganic halide perovskite solar cells (PSCs) have emerged as the most promising third-generation photovoltaic technology due to their high efficiency and low-cost solution-processed device fabrication^{1,2}. Currently, the highest certified power conversion efficiency (PCE) of PSCs has achieved 25.7%, which is comparable with that of silicon solar cells³. Recently, flexible PSCs have gained increasing attention due to their light weight, portability, and adaptability for building-integrated photovoltaics^{4,5}. However, the efficiency and stability of flexible PSCs still lag behind those of rigid PSCs due to low crystallization of perovskite films with more defect sites on flexible substrates⁶. Moreover, the mechanical stability of flexible PSCs is not good enough due to the brittle nature of perovskite film⁷.

Many efforts have been made to enhance the performance of flexible PSCs. Combining 2D perovskite and 3D perovskite to construct 2D/3D heterostructure can enhance the mechanical durability of flexible PSCs⁸. However, the introduction of organic spacer molecules may exert a negative influence on charge transport. The incorporation of polymer additives can significantly enhance the mechanical stability of flexible PSCs. For example, Gao and co-workers introduced β -cyclodextrin (β -CD) and adamantane (AA) as a self-healing system into flexible PSCs, which significantly enhanced the mechanical stability⁹.

Alloying Sn and Pb to get Sn–Pb mixed perovskite is an effective method to tune the bandgap of perovskite, which can be a promising way to achieve the highest PCE of single-junction PSCs predicted by the Shockley–Queisser limit^{10,11}. However, little efforts have been focused on flexible Sn–Pb-mixed PSCs.

In this work, we introduce N,N-dimethyl acrylamide (DMAA) as an additive into Sn–Pb-mixed perovskite film. DMAA can form strong interaction with the precursor solution, leading to enhanced crystallization and reduced defects. Meantime, the cross-linkable DMAA formed by in situ polymerization during thermal annealing can anchor at grain boundaries as flexible scaffolds, which is beneficial for enhanced mechanical stability of the perovskite film. Consequently, the PSCs showed PCEs of 16.44% and 15.44% on rigid and flexible substrates, respectively.

Meanwhile, the flexible PSCs demonstrated excellent mechanical stability, which remained over 80% of the original efficiency after 5000 bending cycles at a radius of 5 mm.

RESULTS AND DISCUSSION

Interactions between perovskite film and DMAA

The Sn–Pb mixed perovskite film with a composition of $\text{FA}_{0.7}\text{MA}_{0.3}\text{Sn}_{0.5}\text{Pb}_{0.5}\text{I}_3$ was prepared by one-step antisolvent method with DMAA as additive. The morphology of the perovskite films with and without DMAA additive was investigated by scanning electron microscopy (SEM) and atomic force microscopy (AFM). As shown in Fig. 1a, b, there is no obvious change in the grain size. Remarkably, the root-mean-square (R_q) of the perovskite film decreased from 34.8 to 16.9 nm after the DMAA modification (Fig. 1d, e). Meantime, the cross-sectional SEM images show that the DMAA-modified perovskite film has fewer grain boundaries (Supplementary Fig. 1). We propose that DMAA can coordinate with perovskite precursor to regulate the film crystallization for retarded crystal growth of Sn-containing perovskite, leading to the formation of smooth perovskite film¹². Then, X-ray diffraction (XRD) was conducted to examine the phase of the perovskite films. As can be seen from Fig. 1c, the characteristic peaks at about 14° and 28° correspond to the (110) and (220) planes of mixed Sn–Pb perovskite¹³, implying that DMAA is not incorporated into the perovskite crystal structure. Moreover, the perovskite film with DMAA shows stronger diffraction intensity and reduced full width at half maximum (FWHM) value, indicating enhanced perovskite crystallization. Figure 1f shows the UV–vis absorption of the perovskite films, and the DMAA-modified perovskite film demonstrated slightly enhanced optical absorption.

DMAA contains C = C bonds, which favors in situ cross-linked polymerization during thermal annealing of perovskite¹⁴. Meantime, the C = O bonds can form interaction with uncoordinated ions in perovskite films (Fig. 2a). The photographs of DMAA before and after cross-linking polymerization are shown in Supplementary Fig. 2, which changed from liquid to transparent solid after

¹Key Laboratory of Flexible Electronics (KLoFE) & Institute of Advanced Materials (IAM), School of Flexible Electronics (Future Technologies), Nanjing Tech University (Nanjing Tech), 211816 Nanjing, China. ✉email: iamjpc@njtech.edu.cn; iamtsqin@njtech.edu.cn

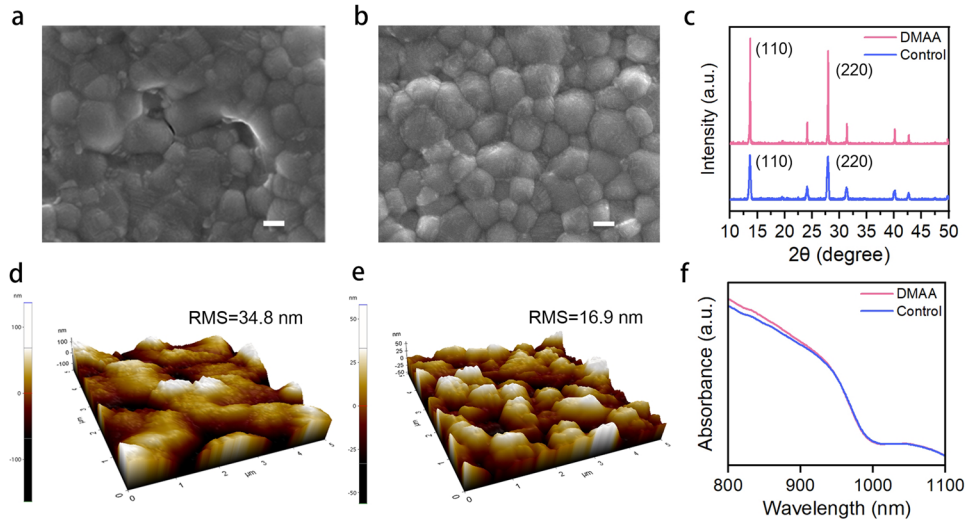


Fig. 1 Morphology, structure, and optical properties of perovskite films. SEM images of perovskite films (a) without and (b) with DMAA, and the scale bar is 100 nm. c XRD patterns of perovskite films. AFM images of perovskite films (d) without and (e) with DMAA. f UV-vis absorption spectra of perovskite films.

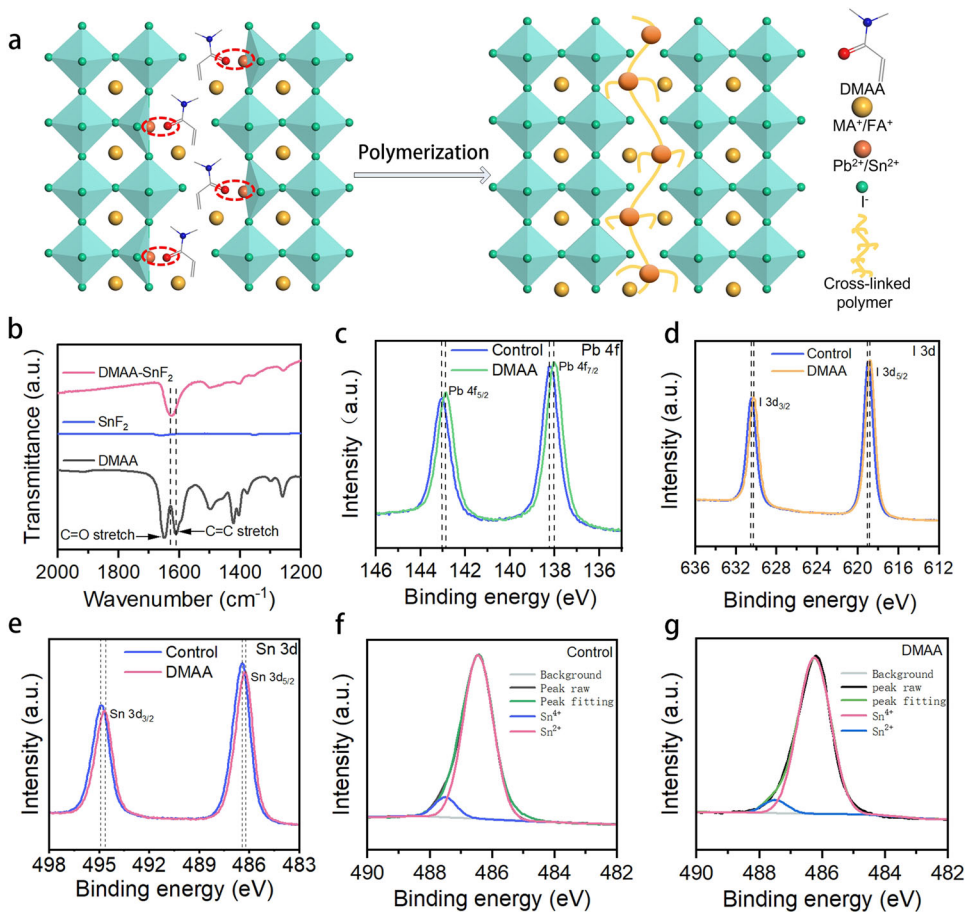


Fig. 2 Interactions between perovskite and DMAA. a Schematic illustration of the interaction between DMAA and perovskite. b FTIR spectra of DMAA, SnF₂ and DMAA-SnF₂ after thermal annealing. XPS spectra of (c) Pb 4f, (d) I 3d, and (e) Sn 3d for the perovskite films. XPS spectra of perovskite film without (f) and with (g) DMAA.

thermal annealing, validating the cross-linking polymerization¹⁵. To study the interaction between DMAA and perovskite, Fourier transform infrared spectra (FTIR) are taken. As shown in Fig. 2b, the C = O peak shifts to lower wavelength, which is resulted from

the coordination of C = O and Sn²⁺¹⁶. Meanwhile, the C = C peak disappeared after thermal annealing, which indicated the cross-linking polymerization¹⁷. To further investigate the interaction between DMAA and perovskite, X-ray photoelectron spectroscopy

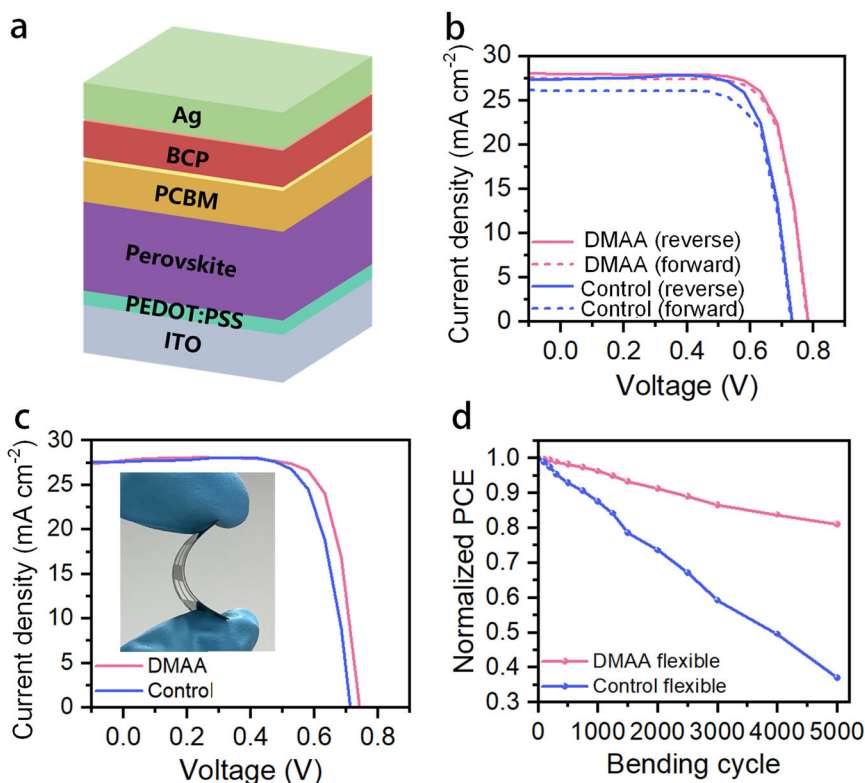


Fig. 3 Photovoltaic performance of Sn–Pb mixed PSCs. **a** Device structure of the Sn–Pb mixed PSCs. **b** J – V curves of the Sn–Pb mixed PSCs on (b) rigid and (c) flexible substrates, the inset of (c) shows the picture of a flexible PSC. **d** Bending tests of flexible PSCs with a bending radius of 5 mm.

(XPS) was conducted and shown in Supplementary Fig. 3 and Fig. 2c–e. Due to the electron-donating nature of the C = O group, the peaks of Pb, Sn, and I shift to lower binding energies after the incorporation of DMAA, indicating the interaction between DMAA and perovskite^{18,19}. Meanwhile, the Sn 3d spectra of the films were deconvoluted into two peaks corresponding to Sn²⁺ and Sn⁴⁺, respectively (Fig. 2f, g). The DMAA-modified perovskite film shows lower Sn⁴⁺ peak than that of the control film, indicating the introduction of DMAA can effectively suppress the oxidation of Sn²⁺, which is beneficial for enhanced photovoltaic performance²⁰. The mitigation of Sn²⁺ oxidation induced by DMAA can be attributed to the smooth perovskite film and the coordination between DMAA and Sn²⁺, which synergistically inhibit oxygen ingressing into the film and improve the oxidation resistance of the film²¹.

Photovoltaic performance of Sn–Pb mixed PSCs

PSCs with a structure of ITO/PEDOT:PSS/perovskite/PCBM/BCP/Ag were fabricated to investigate the effect of DMAA on photovoltaic performance (Fig. 3a). The optimal amount of DMAA in the precursor was obtained by careful optimization, and the photovoltaic parameters of devices with different contents of DMAA are shown in Supplementary Fig. 4. The current density–voltage (J – V) curves of the champion device with and without DMAA are shown in Fig. 3b. The control device showed short-circuit current (J_{SC}) of 27.36 mA cm⁻², open-circuit voltage (V_{OC}) of 0.73 V, fill factor (FF) of 74.94, and a PCE of 15.03%. The device modified with DMAA showed enhanced performance with J_{SC} of 27.79 mA cm⁻², V_{OC} of 0.78 V, and FF of 75.05, yielding a PCE of 16.44%. Importantly, much reduced hysteresis was observed in the DMAA-modified device, which can be ascribed to the enhanced perovskite film quality²². The external quantum efficiency (EQE) spectra of the devices are shown in Supplementary Fig. 5, and the integrated J_{SC}

are in line with the results from the J – V curves. Meantime, the DMAA-modified unencapsulated devices showed excellent long-term stability, which remained more than 90% of the initial efficiency after 1000 h storage in N₂ glovebox (Supplementary Fig. 6). On the other hand, the control device degraded quickly and maintained only 40% of the original efficiency after 500 h. Then, flexible PSCs are prepared and the DMAA-modified devices achieved a PCE of 15.44%, while the control device showed a lower PCE of 14.22% (Fig. 3c). The corresponding statistic photovoltaic parameters are summarized in Supplementary Fig. 7. The bending stability of the devices was evaluated with a curvature radius of 5 mm. As demonstrated in Fig. 3d, the PSCs with DMAA maintained over 80% of the initial efficiency after 5000 bending cycles, while the PCE of the control device gradually decreased to 35% under the same condition. The cross-linking DMAA located at grain boundaries can protect the perovskite films, leading to the enhanced mechanical stability of the devices.

Charge-carrier dynamics

To analyze the carrier kinetics of the perovskite films, steady-state photoluminescence (PL) spectroscopy was taken. As seen in Fig. 4a, the PL intensity of the film with DMAA is higher than that of the control film, indicating improved film quality with reduced non-radiative recombination. Figure 4b shows the dark J – V curve of the devices, and DMAA-modified device has a much lower dark current density than that of the control, indicating that the introduction of DMAA can effectively reduce the leakage current²³. To quantitatively estimate the defects of the perovskite films, the space-charge-limited-current (SCLC) was measured and shown in Fig. 4c. Hole-only devices with the structure of ITO/PEDOT:PSS/perovskite/Au were prepared, and trap density (N_t) can be calculated from $N_t = 2\epsilon\epsilon_0 V_{TF}/qL^2$, where q is the elementary charge, L is the thickness of the perovskite layer, ϵ_0 is the vacuum

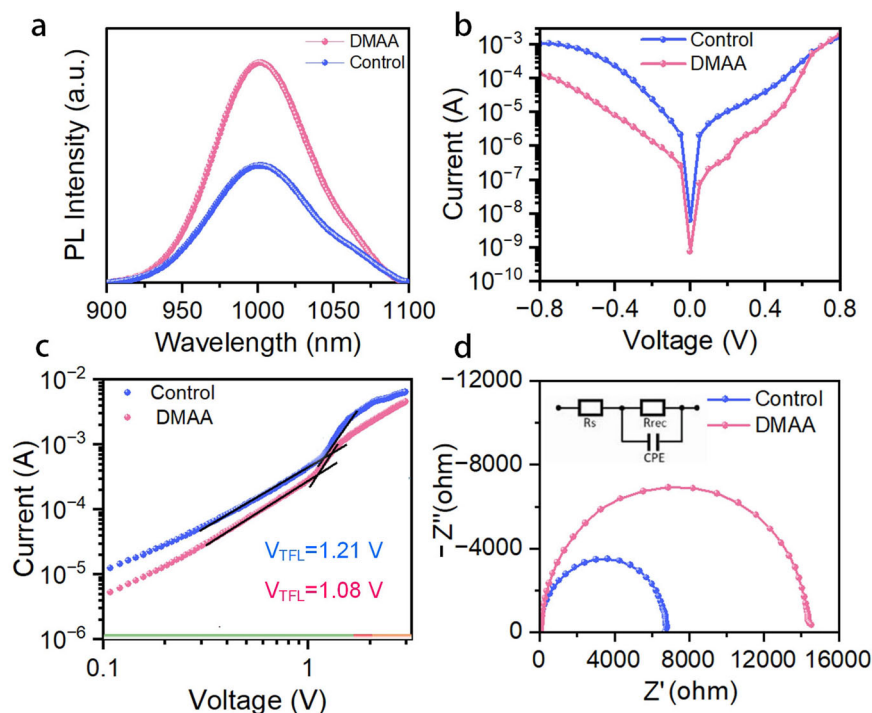


Fig. 4 Charge-carrier dynamics. **a** Steady-state PL spectra of perovskite films. **b** Dark J - V curves of the PSCs. **c** I - V curves of the hole-only devices. **d** Nyquist plots of the PSCs and the inset shows the equivalent circuit diagram used for calculation.

permittivity, ϵ is the dielectric constant of the perovskite film, and V_{TFL} is the trap filling limit voltage^{24,25}. With the DMAA additive, the calculated trap density decreased from $4.34 \times 10^{14} \text{ cm}^{-3}$ to $3.87 \times 10^{14} \text{ cm}^{-3}$, which confirms the defect passivation effect of DMAA. Then, electrical impedance spectroscopy (EIS) was measured to understand the charge transfer process of the PSCs²⁶. The Nyquist plots of devices can be fitted using the equivalent circuit such as the inset in Fig. 4d and the low-frequency arcs of the diagram represent charge recombination resistance²⁷. As shown in Fig. 4d, the device with DMAA shows larger charge recombination resistance, which indicates the DMAA additive can inhibit charge recombination.

In summary, we incorporated DMAA into perovskite film to in situ form cross-linking scaffolds for flexible Sn-Pb mixed PSCs. The DMAA can interact with perovskite precursor to regulate the crystallization process, leading to enhanced crystallinity and reduced defects. In addition, the polymer can chemically anchor at grain boundaries, which can greatly improve the mechanical stability of the devices. Sn-Pb mixed PSCs achieved PCEs of 16.44% and 15.44% on rigid and flexible substrates, respectively. More importantly, the flexible PSCs demonstrated excellent bending stability, which retained over 80% of the initial performance after 5000 bending cycles at a radius of 5 mm. This work provides a promising method for achieving high-performance flexible devices for portable and wearable applications.

METHODS

Materials

Poly(3,4-ethylenedioxythiophene) polystyrene sulfonate (PEDOT:PSS, Clevis PVP Al 4083) was purchased from Heraeus. *N,N*-dimethylformamide (DMF), dimethyl sulfoxide (DMSO), chlorobenzene (CB), tin (II) iodide (SnI_2), lead iodide (PbI_2), tin (II) fluoride (SnF_2), formamidinium iodide (FAI), methylammonium iodide (MAI), were purchased from Sigma-Aldrich. Bathocuproine (BCP) was purchased from TCI.

Device fabrication

ITO-coated substrates were cleaned by ultra-sonication in deionized water, acetone, and isopropyl alcohol for 10 min, respectively. PEDOT:PSS was spin-coated onto ITO substrates at 4000 rpm for 30 s and annealed at 150 °C for 30 min. Then, the substrates were transferred to a nitrogen glovebox. The 1.45 M $\text{FA}_{0.7}\text{MA}_{0.3}\text{Sn}_{0.5}\text{Pb}_{0.5}\text{I}_3$ perovskite precursor solution was prepared in mixed solvents of DMF and DMSO with a volume of 4:1. In total, 10 mol% SnF_2 relative to SnI_2 was added in the precursor solution. In terms of DMAA additive, the molar ratio of DMAA and SnI_2 was 3%, 5%, 10%, and 20%, and the DMAA additive was directly added to the precursor solution. The mixed perovskite solution was spin-coated on PEDOT:PSS layer at 4000 rpm for 30 s, and CB was poured on the film at 10th s, followed by annealing at 100 °C for 10 min. PCBM (20 mg ml⁻¹ in CB) and BCP (0.5 mg ml⁻¹ in IPA) were spin-coated on the perovskite film at 2000 rpm for 30 s and 5000 rpm for 30 s, respectively. Finally, 100 nm Ag was evaporated by thermal evaporation under high vacuum to fabricate PSCs with 0.1-cm² active areas.

Characterization

SEM was performed by JSM-7800F (JEOL, Japan) with a field-emission gun electron source. The perovskite films were first covered with a thin layer of gold before the SEM measurement. The ultraviolet-visible (UV-Vis) absorption spectra were performed on UV-1750 (Shimadzu, Japan). Fourier transform infrared spectroscopy (FTIR) was performed on Scientific Nicolet iS50 (Thermo, America) with ATR Unit. EIS measurement was recorded on CHI760E electrochemical workstation (CH Instruments Ins, USA). J - V curves were measured by using a Class 3A solar simulator (XES-40S3, SAN-EI) under AM 1.5 G standard light equipped with a Keithley 2400 source meter. A shadow mask was used to define the effective aperture area of the device to 0.09 cm². The scanning rate was 100 mV s⁻¹ with a voltage step of 10 mV, using both reverse (from V_{OC} to J_{SC}) and forward (from J_{SC} to V_{OC}) scans. XPS was performed on PHI 5000 VersaProbe III (Ulvac-Phi, Japan) using

Al K α radiation. PL was performed on FLS980 spectrometer by Edinburgh Instruments using a pulsed excitation source at 520 nm with a repetition rate of 1 MHz.

DATA AVAILABILITY

The authors declare that the data supporting the findings of this study are available within the paper and its supplementary information files.

Received: 28 December 2022; Accepted: 16 March 2023;

Published online: 30 March 2023

REFERENCES

- Kojima, A., Teshima, K., Shirai, Y. & Miyasaka, T. Organometal halide perovskites as visible-light sensitizers for photovoltaic cells. *J. Am. Chem. Soc.* **131**, 6050–6051 (2009).
- Green, M. A., Ho-Baillie, A. & Snaith, H. J. The emergence of perovskite solar cells. *Nat. Photon.* **8**, 506–514 (2014).
- NREL Efficiency Chart (2023.01). <https://www.nrel.gov/pv/cell-efficiency.html> (2023).
- Hu, Y. et al. Flexible perovskite solar cells with high power-per-weight: progress, application, and perspectives. *ACS Energy Lett.* **6**, 2917–2943 (2021).
- Zhang, J., Zhang, W., Cheng, H.-M. & Silva, S. R. P. Critical review of recent progress of flexible perovskite solar cells. *Mater. Today* **39**, 66–88 (2020).
- Meng, X. et al. Bio-inspired vertebral design for scalable and flexible perovskite solar cells. *Nat. Commun.* **11**, 3016 (2020).
- Meng, X. et al. Stretchable perovskite solar cells with recoverable performance. *Angew. Chem. Int. Ed.* **59**, 16602–16608 (2020).
- Wang, Z. et al. An embedding 2D/3D heterostructure enables high-performance FA-alloyed flexible perovskite solar cells with efficiency over 20%. *Adv. Sci.* **8**, 2101856 (2021).
- Yang, Z. et al. Self-healing and efficient flexible perovskite solar cells enabled by host–guest interaction and a 2D/3D heterostructure. *J. Mater. Chem. A* **10**, 22445–22452 (2022).
- Shockley, W. & Queisser, H. J. Detailed balance limit of efficiency of p-n junction solar cells. *J. Appl. Phys.* **32**, 510–519 (1961).
- Cao, J. et al. Ultrathin self-assembly two-dimensional metal–organic framework films as hole transport layers in ideal-bandgap perovskite solar cells. *ACS Energy Lett.* **7**, 3362–3369 (2022).
- Zhang, W. et al. Oxalate pushes efficiency of CsPb_{0.7}Sn_{0.3}IBr₂ based all-inorganic perovskite solar cells to over 14%. *Adv. Sci.* **9**, 2106054 (2022).
- Liu, F. et al. Highly efficient and stable self-powered mixed tin-lead perovskite photodetector used in remote wearable health monitoring technology. *Adv. Sci.* **10**, 2205879 (2023).
- Zhang, H. et al. Multifunctional crosslinking-enabled strain-regulating crystallization for stable, efficient α -FAPbI₃-based perovskite solar cells. *Adv. Mater.* **33**, 2008487 (2021).
- Zhao, Y. et al. A polymerization-assisted grain growth strategy for efficient and stable perovskite solar cells. *Adv. Mater.* **32**, 1907769 (2020).
- Takahashi, A. & Hisatomi, H. Hydrophilic monomers suppress the adsorption of plasma protein onto a poly(vinylidene fluoride) membrane. *Mol. Med Rep.* **2**, 749–752 (2009).
- Ma, R. et al. Self-polymerization of monomer and induced interactions with perovskite for highly performed and stable perovskite solar cells. *Adv. Funct. Mater.* **32**, 2105290 (2022).
- Wu, Z. et al. Highly efficient perovskite solar cells enabled by multiple ligand passivation. *Adv. Energy Mater.* **10**, 1903696 (2020).
- Cao, Q. et al. Environmental-friendly polymer for efficient and stable inverted perovskite solar cells with mitigating lead leakage. *Adv. Funct. Mater.* **32**, 2201036 (2022).
- Lim, E. L., Hagfeldt, A. & Bi, D. Toward highly efficient and stable Sn²⁺ and mixed Pb²⁺/Sn²⁺ based halide perovskite solar cells through device engineering. *Energy Environ. Sci.* **14**, 3256–3300 (2021).

- Li, G. et al. Ionic liquid stabilizing high-efficiency tin halide perovskite solar cells. *Adv. Energy Mater.* **11**, 2101539 (2021).
- Kim, H.-S. & Park, N.-G. Parameters affecting I–V hysteresis of CH₃NH₃PbI₃ perovskite solar cells: effects of perovskite crystal size and mesoporous TiO₂ layer. *J. Phys. Chem. Lett.* **5**, 2927–2934 (2014).
- Wang, J. et al. Carbazole-based hole transport polymer for methylammonium-free tin–lead perovskite solar cells with enhanced efficiency and stability. *ACS Energy Lett.* **7**, 3353–3361 (2022).
- Xu, G. et al. Integrating ultrathin bulk-heterojunction organic semiconductor intermediary for high-performance low-bandgap perovskite solar cells with low energy loss. *Adv. Funct. Mater.* **28**, 1804427 (2018).
- Jiang, T. et al. Realizing high efficiency over 20% of low-bandgap Pb–Sn-alloyed perovskite solar cells by in situ reduction of Sn⁴⁺. *Sol. RRL* **4**, 1900467 (2020).
- Lee, S. et al. Inorganic narrow bandgap CsPb_{0.4}Sn_{0.6}I_{2.4}Br_{0.6} perovskite solar cells with exceptional efficiency. *Nano Energy* **77**, 105309 (2020).
- Lin, Q., Armin, A., Nagiri, R. C. R., Burn, P. L. & Meredith, P. Electro-optics of perovskite solar cells. *Nat. Photon.* **9**, 106–112 (2015).

ACKNOWLEDGEMENTS

This work was funded financially by the National Natural Science Foundation of China (62204114, 62075094, 62205143); Natural Science Foundation of Jiangsu Province (BK20211537).

AUTHOR CONTRIBUTIONS

J.C. and T.Q. planned and supervised the project. Y.L. conducted most of the experiments. S.Y., H.C., B.L., J.X., and Y.S. supported the experiments. All authors analyzed the data and discussed the manuscript.

COMPETING INTERESTS

The authors declare no competing interests.

ADDITIONAL INFORMATION

Supplementary information The online version contains supplementary material available at <https://doi.org/10.1038/s41528-023-00253-4>.

Correspondence and requests for materials should be addressed to Jiupeng Cao or Tianshi Qin.

Reprints and permission information is available at <http://www.nature.com/reprints>

Publisher's note Springer Nature remains neutral with regard to jurisdictional claims in published maps and institutional affiliations.



Open Access This article is licensed under a Creative Commons Attribution 4.0 International License, which permits use, sharing, adaptation, distribution and reproduction in any medium or format, as long as you give appropriate credit to the original author(s) and the source, provide a link to the Creative Commons license, and indicate if changes were made. The images or other third party material in this article are included in the article's Creative Commons license, unless indicated otherwise in a credit line to the material. If material is not included in the article's Creative Commons license and your intended use is not permitted by statutory regulation or exceeds the permitted use, you will need to obtain permission directly from the copyright holder. To view a copy of this license, visit <http://creativecommons.org/licenses/by/4.0/>.

© The Author(s) 2023